

Finite time quantum-classical correspondence in quantum chaotic systems

Qian Wang

*CAMTP-Center for Applied Mathematics and Theoretical Physics,
University of Maribor, Mladinska 3, SI-2000 Maribor, Slovenia, and
Department of Physics, Zhejiang Normal University, Jinhua 321004, China*

Marko Robnik

*CAMTP-Center for Applied Mathematics and Theoretical Physics,
University of Maribor, Mladinska 3, SI-2000 Maribor, Slovenia*

(Dated: September 10, 2024)

Although the importance of the quantum-classical correspondence has been recognized in numerous studies of quantum chaos, whether it still holds for finite time dynamics remains less known. We address this question in this work by performing a detailed analysis of how the quantum chaotic measure relates to the chaoticity of the finite time classical trajectories. A good correspondence between them has been revealed in both time dependent and many-body systems. In particular, we show that the dependence of the quantum chaotic measure on the chaoticity of finite time trajectories can be well captured by a function that is independent of the system. This strongly implies the universal validity of the finite time quantum-classical correspondence. Our findings provide a deeper understanding of the quantum-classical correspondence and highlight the role of time for studying quantum ergodicity.

I. INTRODUCTION

Since the beginning of the quantum theory, the quantum-classical correspondence principle has attracted countless investigations and remains an interesting topic in current researches. Roughly speaking, it states that there should be an agreement between the quantum and classical predictions in certain classical limit. There are several formulations of the quantum-classical correspondence principle [1–4]. Among them, the most famous one is the Bohr’s corresponding principle [1, 2], which plays a crucial role for interpretation of quantum mechanics. Although the quantum-classical correspondence principle has been verified in abundant literature, see e. g. Refs. [5–12], it meets several difficulties in the studies of quantum chaos.

On the one hand, it is known that the energy spectrum of any bounded quantum system is discrete. As a result, the quantum motion should always be governed by the regular dynamics, rather than the chaotic one, which appears for the continuous spectrum. However, this is in conflict with the observed classical dynamical chaos [13] and indicates the failure of the traditional quantum-classical correspondence. In fact, the chaotic behavior exhibited in the system with discrete spectrum requires us to modify the quantum-classical correspondence principle by considering the finite time behavior. On the other hand, different from the classical systems, the Heisenberg uncertainty relation leads to a finite resolvable limit in the phase space of quantum systems. This further suppresses the quantum chaotic motion to agree with its classical counterpart [14]. Moreover, the quantum interference effect among the phase space structures of quantum systems gives rise to localization phenomena even in strongly chaotic systems. Consequently, the quantum chaotic systems with well-defined classical limit could allow their spectral statistics to exhibit significant deviations from the expected Wigner-Dyson statistics [15–19]. Additionally, the extremely slow diffusion dynamics in classical systems [20–24] provides an alternative mechanism that leads to the breakdown of the quantum-classical correspondence in the finite time.

All these facts together raise an intriguing question of whether the quantum-classical correspondence still holds for the finite time motion. A very recent work performed by Casati and coworkers has explored this question in several billiards [25]. By associating the finite time classical trajectories with a certain energy shell of the quantum system, a well-defined correspondence between the quantum and classical chaotic measures has been established in their studies. This provides an evidence of the validity of the quantum-classical correspondence in the finite time dynamics. However, a general conclusion remains elusive, since the billiards are the single body systems. Hence, it is necessary to investigate the finite time quantum-classical correspondence in different quantum systems, particularly the many-body systems, to enhance the conclusion in above mentioned study.

In this work, utilizing the concepts proposed in Ref. [25], we carry out a detailed investigation of the finite time quantum-classical correspondence in two quantum systems that are distinct from the billiards. The first one is the kicked top model, a prototypical model for studying of quantum chaos [26]. Although the kicked top model is also a single particle system, it has time-dependent Hamiltonian that distinguishes it from the billiards. The second system is a many-body system, namely the well-known Dicke model [27], which has a smooth classical Hamiltonian limit, in general of the mixed type classical dynamics. Different from both billiards and kicked top model, the classical

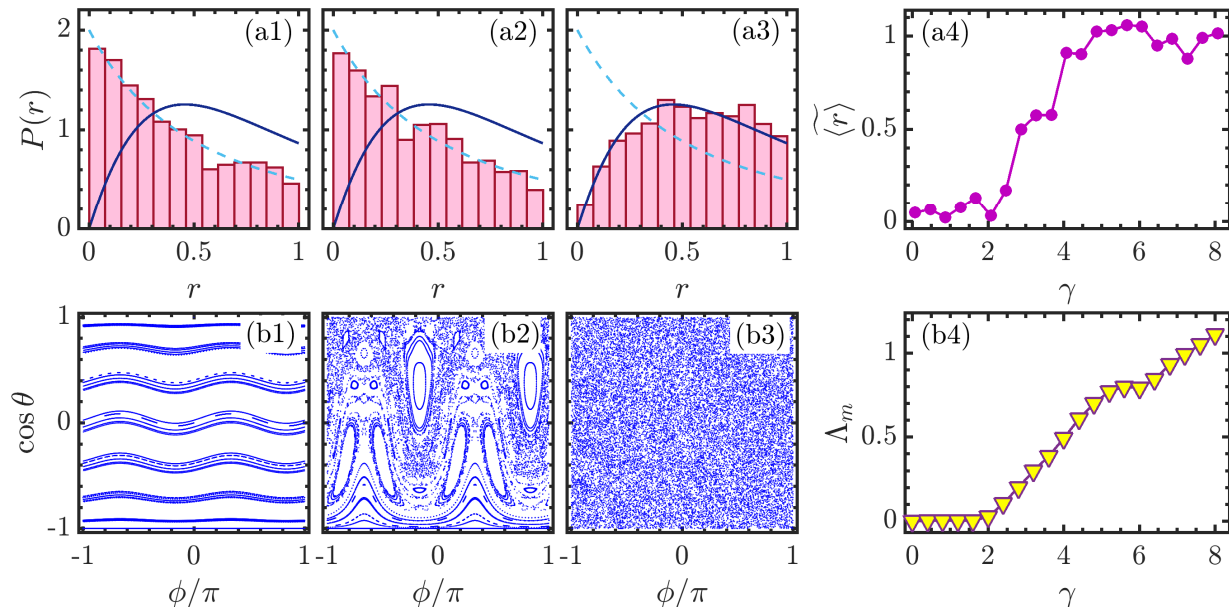


FIG. 1. (a1)-(a3): Level spacing ratio probability distribution in Eq. (3) of the KT model for $\gamma = 0.2$ (a1), $\gamma = 2.3$ (a2), and $\gamma = 7$ (a3) with $j = 2000$. The dashed and solid curves in each panel denote $P_P(r)$ and P_{WD} in (4), respectively. (a4) Averaged ratio $\langle \tilde{r} \rangle$ [cf. Eq. (5)] of the KT model as a function of γ for $j = 2000$. (b1)-(b3): Classical phase space portraits of the KT model for 90 random initial conditions with $\gamma = 0.2, 2.3$, and $\kappa = 7$ [from (b1) to (b3)]. Each initial condition has been evolved for 300 kicks. (b4) Phase space averaged Lyapunov exponent Λ_m (7) of the KT model as a function of γ . Here, Λ_m is numerically obtained by averaging over 2×10^4 initial conditions, each evolved for 1×10^5 kicks. Other parameter: $\beta = \pi/3$.

dynamics of the Dicke model is governed by differential equations, rather than the mapping.

By employing the Poincaré section, we show how to define the classical chaotic measure for a finite time classical trajectory. We demonstrate that the classical chaoticity quantified by finite time trajectories exhibits a good agreement with the quantum chaoticity. In particular, we find that the dependence between the quantum and classical chaotic measures of totally different systems can be captured by the same function. This remarkable finding not only extends the previous results in Ref. [25] to more general systems, but also promotes our understanding of the quantum-classical correspondence principle. In addition, it further implies the existence of a universal relationship between the quantum and finite time classical chaotic measures.

The rest of this article is organized as follows. In Sec. II, we first introduce the kicked top model and then report on our numerical results of the finite time quantum-classical correspondence. The Sec. III is devoted to the study of a different model, the Dicke model. Here, we show that the numerical results obtained from the Dicke model are similar to the kicked top model, suggesting the universality of the finite time quantum-classical correspondence. We finally summarize our findings in Sec. IV with several remarks.

II. KICKED TOP MODEL

The kicked top (KT) model [26, 28], firstly introduced in the context of quantum chaos [29–38], describes the periodic kicking on a precessing top with angular momentum $\mathbf{J} = (J_x, J_y, J_z)$. This model has been extensively studied in many areas of physics [39–49] and can be realized in different experimental platforms [50–52]. The Hamiltonian of the KT model can be written as

$$H_{KT} = \beta J_z + \frac{\gamma}{2j} J_x^2 \sum_{n=-\infty}^{+\infty} \delta(t - n), \quad (1)$$

where β is the angular frequency of the precession around z axis, γ denotes the strength of the δ kicks with unit period, and j quantifies the total magnitude of \mathbf{J} , so that $\mathbf{J}^2 = j(j+1)$. Here, we set $\hbar = 1$ throughout this work.

The conservation of \mathbf{J}^2 in the KT model allows us to work in the Dicke basis $|j, m\rangle$, defined by $j_z |j, m\rangle = m |j, m\rangle$ and $\mathbf{J}^2 |j, m\rangle = j(j+1) |j, m\rangle$ with $-j \leq m \leq j$, and the dimension of the Hilbert space is $\mathcal{D} = 2j + 1$. Moreover, the

Hamiltonian (1) also conserves the parity operator $\Pi = (-1)^{(j+J_z)}$. Consequently, the Hilbert space can be further split into even- and odd-parity subspaces with dimensions $\mathcal{D}_e = j + 1$ and $\mathcal{D}_o = j$ for even j . We focus on the even-parity subspace in this work and consider j even.

It is known that the KT model exhibits a transition to chaos with increasing the kick strength [26, 37, 53–55]. The onset of chaos in the KT model can be analyzed through the spectral properties of the Floquet operator, which can be written as

$$\mathcal{F} = \exp\left(-i\frac{\gamma}{2j}J_x^2\right) \exp(-i\beta J_z). \quad (2)$$

By numerically diagonalizing \mathcal{F} in the Dicke basis, we obtain its eigenvalues $\{\alpha_k\} \in [-\pi, \pi)$, also known as the quasienergies of the KT model. Then, we consider the level spacing ratios [56], defined as

$$r_k = \min\left(\delta_k, \frac{1}{\delta_k}\right), \quad (3)$$

where $\delta_k = d_{k+1}/d_k$ with $d_{k+1} = \alpha_{k+1} - \alpha_k$ being the spacing between two nearest quasienergies. The presence of chaos can be revealed by the probability distribution of r_k , denoted by $P(r)$. It has been verified that for the regular and fully chaotic systems $P(r)$ are, respectively, captured by the Poisson and Wigner-Dyson distributions [57–59],

$$P_P = \frac{2}{(1+r)^2}, \quad P_{WD} = \frac{27}{4} \frac{r+r^2}{(1+r+r^2)^{5/2}}. \quad (4)$$

In Figs. 1(a1)-1(a3), we plot how $P(r)$ varies as γ is increased. The crossover from $P_P(r)$ to $P_{WD}(r)$ with increasing γ is clearly visible, indicating the occurrence of chaos at larger values of γ . Further confirmation of the transition to chaos is provided by the rescaled average ratio, defined by [37]

$$\widetilde{\langle r \rangle} = \frac{|\langle r \rangle - \langle r \rangle_P|}{\langle r \rangle_{WD} - \langle r \rangle_P}. \quad (5)$$

Here, $\langle r \rangle$ is the average of r_k , $\langle r \rangle_P = \int r P_P(r) dr \approx 0.39$, and $\langle r \rangle_{WD} = \int r P_{WD}(r) dr \approx 0.53$ [57]. The results in Figs. 1(a1)-1(a3) suggest that $\widetilde{\langle r \rangle}$ keeps its value around the zero for smaller values of γ , while it saturates near $\widetilde{\langle r \rangle} \approx 1$ when γ is sufficient large. This is displayed in Fig. 1(a4), where the dependence of $\widetilde{\langle r \rangle}$ on γ is shown.

The transition to chaos in (1) can be considered as a quantum manifestation of the chaotic motion in its classical counterpart. The classical KT model is described by the following classical map [37]

$$\begin{bmatrix} X_{n+1} \\ Y_{n+1} \\ Z_{n+1} \end{bmatrix} = \begin{pmatrix} \cos \beta & -\sin \beta & 0 \\ \sin \beta \cos \Theta_n & \cos \beta \cos \Theta_n & -\sin \Theta_n \\ \sin \beta \sin \Theta_n & \sin \beta \sin \Theta_n & \cos \Theta_n \end{pmatrix} \begin{bmatrix} X_n \\ Y_n \\ Z_n \end{bmatrix}, \quad (6)$$

where $\Theta_n = \gamma(X_n \cos \beta - Y_n \sin \beta)$. The classical vector $\mathbf{X} = (X, Y, Z)$ satisfies $|\mathbf{X}|^2 = X^2 + Y^2 + Z^2 = 1$. We thus parametrize (X, Y, Z) as $X = \sin \theta \cos \phi$, $Y = \sin \theta \sin \phi$ and $Z = \cos \theta$, with θ, ϕ being the azimuthal and polar angles, respectively. The classical phase space is characterized by canonical variables $\phi = \arctan(Y/X)$ and $\cos \theta$.

The classical phase portraits for several kick strengths are plotted in Figs. 1(b1)-1(b3). As γ is increased, the phase space evolves from occupied by regular orbits ($\gamma = 0.2$) to the celebrated Kolmogorov-Arnold-Moser scenario ($\gamma = 2.3$), and to the almost entirely covered by chaotic trajectories, with invisible regular islands ($\gamma = 7$). These observed features can be quantitatively captured by the phase space averaged Lyapunov exponent, defined by

$$\Lambda_m = \frac{1}{4\pi} \int \lambda_m \sin \theta d\theta d\phi. \quad (7)$$

Here, λ_m is the largest Lyapunov exponent of the classical map (6) and it can be calculated as [29, 60] $\lambda_m = \ln[\lim_{n \rightarrow \infty} (\tau_m)^{1/n}]$ with τ_m being the maximal eigenvalue of $\mathcal{T} = \prod_{s=1}^n (\partial \mathbf{X}_{s+1} / \partial \mathbf{X}_s)$. The variation of Λ_m as a function of γ is shown in Fig. 1(b4). It is obvious that Λ_m remains zero for $\gamma \lesssim 2$, due to the regularity of the model. However, it grows with increasing γ as soon as $\gamma > 2$, indicating the onset of chaos in the model. Here, it is worth mentioning that even though the transition to chaos in the KT model depends on the value of β [61], the main results of this work are independent of it. This has been carefully checked in our studies. We thus fixed $\beta = \pi/3$ in the present work.

By comparing Fig. 1(a4) with 1(b4), we note that the upturns in $\widetilde{\langle r \rangle}$ and Λ_m are in agreement with each other, suggesting a good quantum-classical correspondence. This is however expected in the infinite time limit, whether it still holds for finite time case remains unknown. In the rest of this section, we address this question in the KT model by exploring how the classical chaotic measure, defined through the finite time trajectories, relates to the degree of quantum chaos.

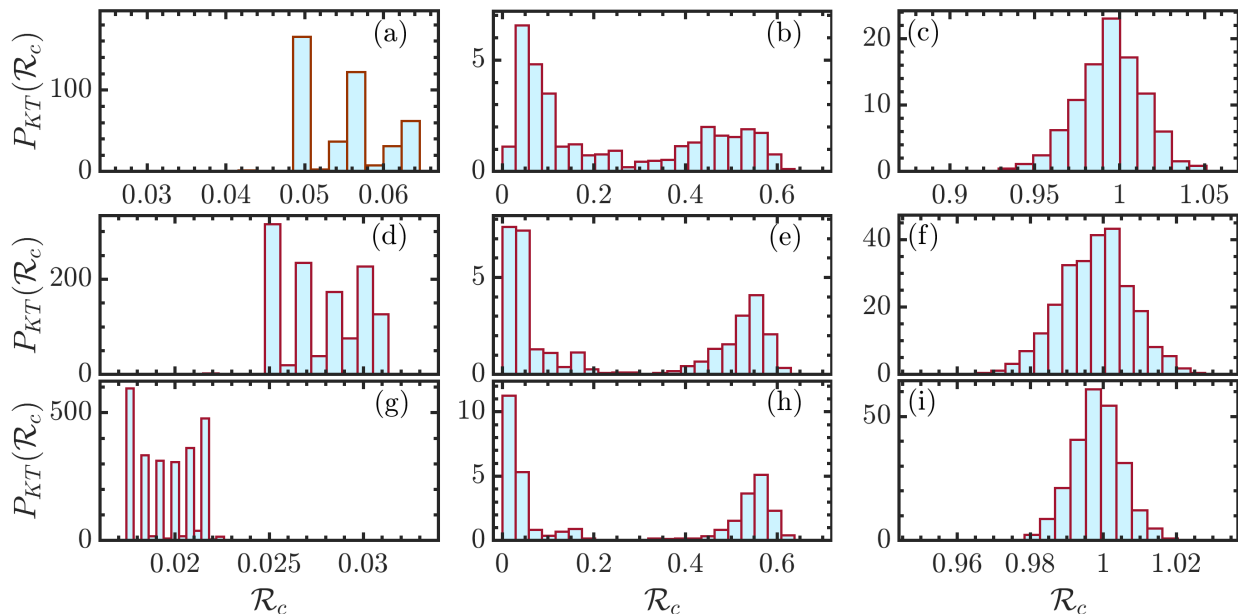


FIG. 2. (a)-(c): Probability distribution, $P_{KT}(\mathcal{R}_c)$, of \mathcal{R}_c in Eq. (9) for $\gamma = 0.2$ (a), $\gamma = 2.3$ (b) and $\gamma = 7$ (c) with $N_k = 1000$. (d)-(f): $P_{KT}(\mathcal{R}_c)$ for the same values of γ as in panels (a)-(c) with $N_k = 4000$. (g)-(i): $P_{KT}(\mathcal{R}_c)$ for the same γ values as in panels (a)-(c) with $N_k = 8000$. Here, an ensemble of 1600 initial conditions has been employed to calculate the probability distribution $P_{KT}(\mathcal{R}_c)$. Other parameter: $\beta = \pi/3$.

A. Dynamical chaos in KT model

The aim of our studying requires us to quantify the degree of chaos for a given finite time trajectory. To this end, we focus on a classical trajectory evolved for N_k kicks. As a result, a finite time trajectory is described by N_k points in the classical phase space. The distribution of these N_k points in the phase space is strongly dependent on whether the classical dynamics is regular or chaotic. For regular dynamics, N_k points should exhibit clustering and distribute with certain structures in the phase space. In contrast, the chaotic dynamics results in N_k points being randomly scattered, leading to a structureless phase space.

To quantitatively capture above features exhibited by a finite time classical trajectory, we divide the phase space into M_c cells with equal size, and consider the number of occupied cells M_p . Obviously, too small and/or too large value of M_c are not allowed, as they will wipe out the difference between the regular and chaotic dynamics. The suitable value of M_c can be determined via the approach proposed by Casati and coworkers [25]. According to their method, we need to define the Shannon entropy for a certain cell. As an arbitrary cell is either occupied or not occupied, the Shannon entropy of a cell can be defined as

$$S_e(M_c) = -p \ln p - (1-p) \ln(1-p). \quad (8)$$

Here, $p = 1 - (1 - 1/M_c)^{N_k}$ is the occupation probability of our considered cell for N_k points that are randomly distributed over M_c cells. Then, by maximizing the Shannon entropy with respect to M_c , one can find that the optimal value of M_c is given by $M_c = N_k / \ln 2 \approx N_k$. In the numerical simulation, one can take $M_c = N_k$ and define the measure of chaoticity of a finite time trajectory as

$$\mathcal{R}_c = \frac{M_r}{N_k}, \quad (9)$$

where $M_r = M_p / (p M_c) N_k$ is the normalized M_p . One can expect that \mathcal{R}_c will have vanishingly small values for regular trajectories, while it has the order of magnitude $O(1)$ for the chaotic trajectories.

We find that \mathcal{R}_c in (9) indeed enables us to quantify the degree of chaos of the finite time trajectories, as confirmed by its probability distribution for an ensemble of initial conditions, defined by

$$P_{KT}(\mathcal{R}_c) = \frac{1}{N_s} \sum_{u=1}^{N_s} \delta(\mathcal{R}_c - \mathcal{R}_{c,u}), \quad (10)$$

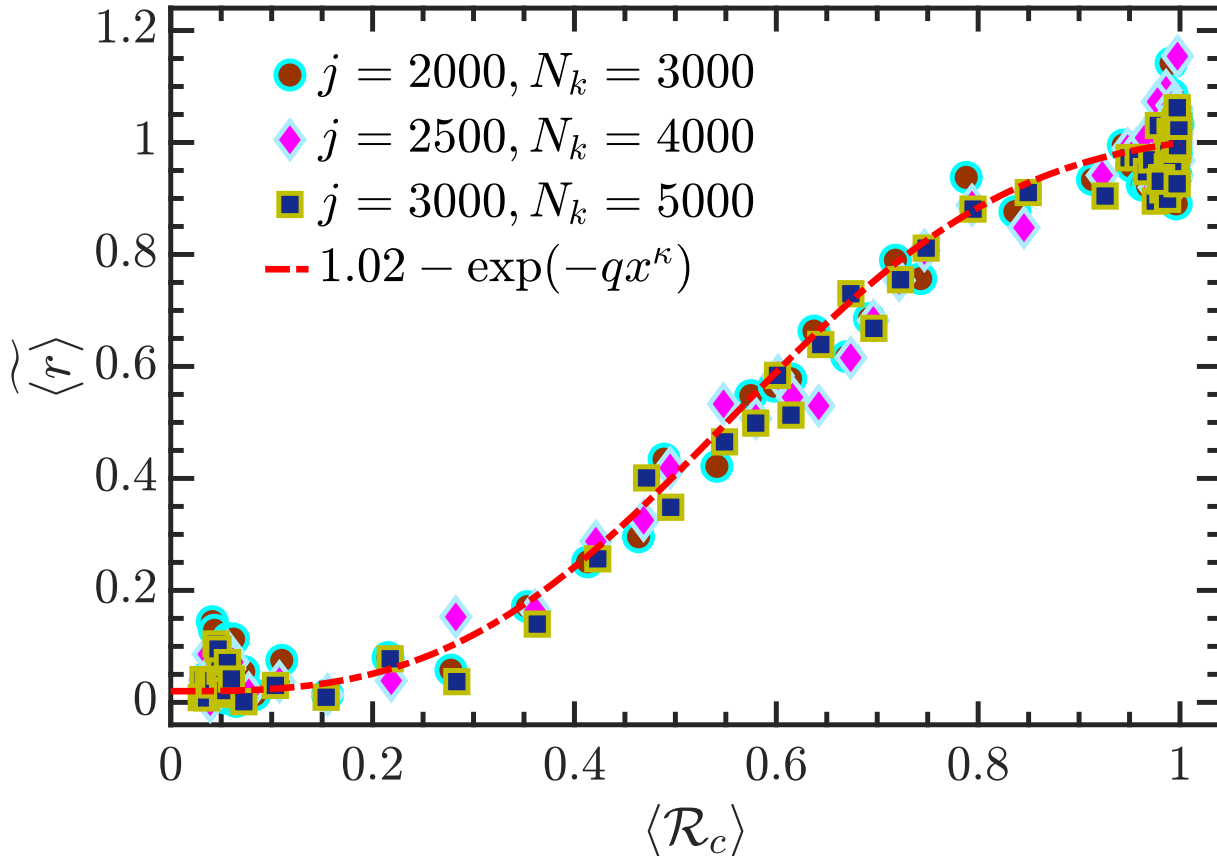


FIG. 3. Quantum chaotic measure $\langle \widetilde{r} \rangle$ in (5) as a function of the finite time classical chaotic measure $\langle \mathcal{R}_c \rangle$ in (11) for the KT model with several values of j and N_k . Here, $\langle \mathcal{R}_c \rangle$ is calculated by averaging over an ensemble with 1600 initial conditions. The red dot-dashed curve denotes the best fitting of the data and it has the form $y = 1.02 - \exp(-qx^\kappa)$ with $\kappa \approx 2.9892$ and $q \approx 3.8834$. Other parameter: $\beta = \pi/3$.

where \mathcal{N}_s is the number of initial conditions in the given ensemble. The regular behavior for the classical trajectories gives rise to vanishingly small values of \mathcal{R}_c , as both the average and fluctuation of $P_{KT}(\mathcal{R}_c)$ are tiny, while the chaotic trajectories would result in a narrow distribution $P_{KT}(\mathcal{R}_c)$ around $\mathcal{R}_c \simeq 1$.

In Fig. 2, we show how $P_{KT}(\mathcal{R}_c)$ varies for several values of γ and N_k . On the one hand, as seen in the first column of Fig. 2, $P_{KT}(\mathcal{R}_c)$ has small average value and width in the regular regime, regardless of the number of kicks. Moreover, we see that the average and width of $P_{KT}(\mathcal{R}_c)$ decrease with increasing N_k . We thus expect that $P_{KT}(\mathcal{R}_c)$ will become a delta distribution located at $\mathcal{R}_c = 0$ in the limit $N_k \rightarrow \infty$. On the other hand, in the chaotic case, the distribution $P_{KT}(\mathcal{R}_c)$ exhibits a concentration with an average value close to 1, as demonstrated in the last column of Fig. 2. Similar to the regular case, the width of $P_{KT}(\mathcal{R}_c)$ for the chaotic trajectories also decreases when we increase N_k . In the limit $N_k \rightarrow \infty$, one can expect that $P_{KT}(\mathcal{R}_c)$ will take the form $P_{KT}(\mathcal{R}_c) = \delta(\mathcal{R}_c - 1)$. For the mixed regime, as shown for the case of $\gamma = 2.3$ in the second column of Fig. 2, the distribution $P_{KT}(\mathcal{R}_c)$ is characterized by double peak shape. Two peaks in $P_{KT}(\mathcal{R}_c)$ are, respectively, corresponding to the regular and chaotic trajectories. We further note that the smoothness of $P_{KT}(\mathcal{R}_c)$ is enhanced by increasing N_k .

Above features of $P_{KT}(\mathcal{R}_c)$ justify the correctness of \mathcal{R}_c for measuring the chaoticity of the finite time classical trajectories. They also imply that the degree of chaos for classical KT model in a finite time can be quantified by the average of \mathcal{R}_c , defined by

$$\langle \mathcal{R}_c \rangle = \sum_u \mathcal{R}_{c,u} P_{KT}(\mathcal{R}_c). \quad (11)$$

To see whether the quantum-classical correspondence still holds in finite time, we examine the dependence between $\langle \mathcal{R}_c \rangle$ and the measure of quantum chaos, given by $\langle \widetilde{r} \rangle$ in Eq. (5). In Fig. 3, we show how $\langle \widetilde{r} \rangle$ correlates with $\langle \mathcal{R}_c \rangle$

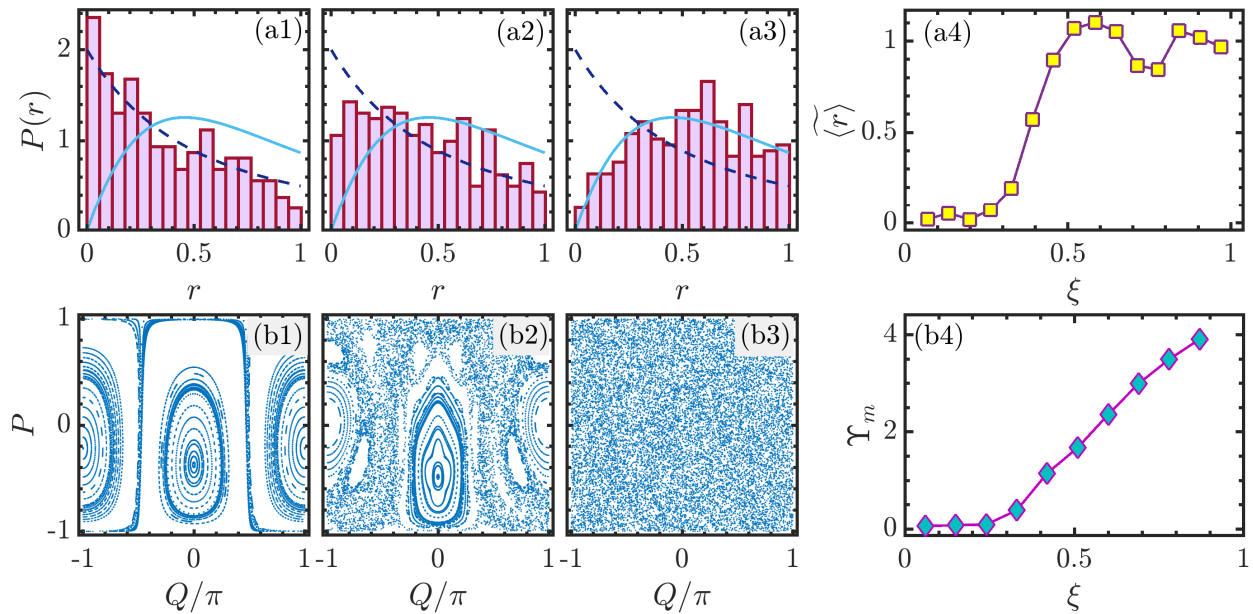


FIG. 4. (a1)-(a3): Probability distribution, $P(r)$, of the level spacing ratio (3) of the Dicke model for $\xi = 0.1$ (a1), $\xi = 0.3$ (a2), and $\xi = 1$ (a3) and energy levels $E_k \in [1.05, 1.22]$ with $N = 80$. The dashed and solid curves in each panel denote $P_P(r)$ and P_{WD} in (4), respectively. (a4) Rescaled averaged ratio $\langle \widetilde{r} \rangle$ in (5) of the Dicke model for the energy levels $E_k \in [1.05, 1.22]$ as a function of ξ with $N = 80$. (b1)-(b3): Classical Poincaré sections in (P, Q) plane of the Dicke model for 81 random initial conditions with $\xi = 0.1, 0.3$, and $\xi = 1$ [from (b1) to (b3)] and a fixed energy $\mathcal{E} = 1.2$. Each initial condition has been evolved for $t = 3000$. (b4) Phase space averaged Lyapunov exponent Υ_m (7) of the Dicke model as a function of ξ . Here, Υ_m is numerically obtained by averaging over 5000 initial conditions, each evolved for $t = 1 \times 10^3$. Other parameters: $\omega = \omega_0 = 1$.

for different values of j and N_k . The collapse of data is clearly visible, indicating that the behavior of $\langle \widetilde{r} \rangle$ is in good agreement with $\langle \mathcal{R}_c \rangle$. In particular, a numerical fitting shows that the variation of $\langle \widetilde{r} \rangle$ with $\langle \mathcal{R}_c \rangle$ can be well captured by a function of the form

$$y = 1.02 - \exp(-qx^\kappa), \quad (12)$$

which has been plotted as the red dot-dashed curve in Fig. (3). For the KT model, we have found that $\kappa \simeq 2.9892$ and $q \simeq 3.8834$ are independent of the values of j and N_k .

These results not only verify the usefulness of \mathcal{R}_c for measuring the chaoticity of the finite time trajectories, but also reveal that the quantum-classical correspondence still holds for the finite time case. However, as the KT model is a single particle system, further investigation of quantum many-body systems is required in order to strengthen above statement. We thus proceed to perform an analysis in the celebrated Dicke model.

III. DICKE MODEL

The Dicke model consists of an ensemble of N spin-1/2 atoms interacting with a single bosonic mode [27, 62] and plays a fundamental role in a wide range of fields, including various phase transitions [63–76], quantum chaos and thermalization [76–89], and information scrambling [90, 91]. It has also been applied to understand several critical phenomena observed in different experimental platforms [92–94]. A very recent review on the properties and applications of the Dicke model can be found in Ref. [95].

The Hamiltonian of the Dicke model can be written as

$$H_D = \omega a^\dagger a + \omega_0 J_z + \frac{2\xi}{\sqrt{N}} (a + a^\dagger) J_x, \quad (13)$$

where ω , ω_0 , and ξ correspond to the frequency of the bosonic mode, energy splitting of atoms, and the strength of atom-field interaction. The bosonic annihilation (creation) operator is denoted by a (a^\dagger), while J_a ($a = x, y, z$) are the collective spin-1/2 operators along a axis and satisfy the SU(2) commutation relations.

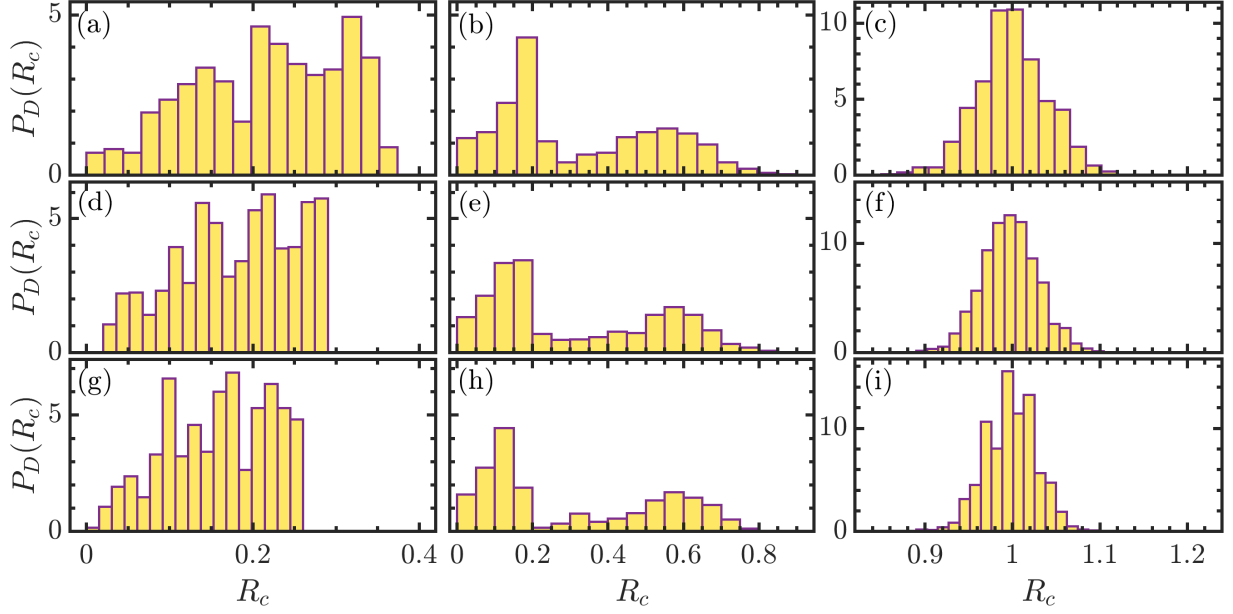


FIG. 5. (a)-(c): Probability distribution, $P_D(R_c)$, of R_c in Eq. (19) for $\xi = 0.1$ (a), $\xi = 0.3$ (b) and $\xi = 1$ (c) with $T_m = 1000$. (d)-(f): $P_D(R_c)$ for the same values of ξ as in panels (a)-(c) with $T_m = 1500$. (g)-(i): $P_D(R_c)$ for the same ξ values as in panels (a)-(c) with $T_m = 2000$. Here, T_m denotes the evolution time of our considered trajectories and an ensemble of 1600 initial conditions has been employed to calculate the probability distribution $P_D(R_c)$. Other parameters: $\omega = \omega_0 = 1$ and the traversal time $T_r \simeq 6.2$.

As the Hamiltonian H_D (13) commutes with $\mathbf{J}^2 = \sum_a J_a^2$, one can divide the Hilbert space into different subspaces distinguished by the eigenvalues of \mathbf{J}^2 , given by $j(j+1)$. We restrict ourselves in the subspace with $j = N/2$ and the dimension of the Hilbert space is $\mathcal{D} = (N+1)(\mathcal{N}_{tr}+1)$ with \mathcal{N}_{tr} being the truncation number of the bosonic mode. Moreover, the conservation of the parity $\Pi = (-1)^{j+J_z+a^\dagger a}$ for H_D enables us to further separate the Hilbert space into even- and odd-parity subspaces. In this work, we focus on the even-parity subspace, so that the dimension of the Hilbert is given by $\mathcal{D}_e = (N/2+1)(\mathcal{N}_{tr}+1) - \mathcal{N}_{tr}/2$ for even N . The requirement of the convergence of the numerical results leads us to take $\mathcal{N}_{tr} = 380$. We have carefully checked that our results are unchanged for increasing \mathcal{N}_{tr} .

Several interesting features have been found in the Dicke model. Among them, the transition to chaos is an intriguing topic and has been triggering many endeavors to explore it, from both static [76, 80–82, 96, 97] and dynamical aspects [84, 91, 98–101]. Generally speaking, the spectral statistics of H_D turns from the Poisson statistics to the Wigner-Dyson statistics around $\xi_c \simeq \sqrt{\omega_0 \omega}/2$. However, a detailed study reveals that the precise value of ξ_c also strongly depends on the energy [82, 85, 102].

In Figs. 4(a1)-4(a3), we show how the distribution of level spacing ratio r_k in (3), $P(r)$, varies with increasing ξ for the energies $E_k \in [\bar{E} - 0.15, \bar{E} + 0.02]$ with $\bar{E} = 1.2$ and the system size $N = 80$. We see that $P(r)$ undergoes an obvious crossover from the Poisson distribution to the Wigner-Dyson distribution as ξ is increased, suggesting the onset of chaos at larger values of ξ . Moreover, as we focus on the energy levels with higher energies, $P(r)$ displays a visible deviation from $P_P(r)$ at $\xi < \sqrt{\omega_0 \omega}/2$, as observed in Fig. 4(a2). The transition to chaos with increasing ξ is more clearly revealed by the upturn in the rescaled averaged level spacing ratio $\langle \tilde{r} \rangle$ around $\xi \sim 0.2$, as seen in Fig. 4(a4).

As in the KT model, the presence of chaos in H_D can be understood as a quantum analogue of the classical chaos. The classical counterpart of the Dicke model is obtained by calculating the expectation value of H_D in the tensor product state $|CS\rangle = |\alpha\rangle \otimes |z\rangle$ [103]. Here, $|\alpha\rangle$ and $|z\rangle$ are the Glauber and Bloch coherent states, defined by [104]

$$|\alpha\rangle = e^{-|\alpha|^2} e^{\alpha a^\dagger} |0\rangle, \quad |z\rangle = \frac{1}{(1+|z|^2)^j} e^{z J_+} |j, -j\rangle, \quad (14)$$

where $\alpha, z \in \mathbb{C}$, $|0\rangle$ is the vacuum state of the bosonic mode, $J_+ = J_x + iJ_y$, and $|j, -j\rangle$ fulfills $J_z |j, -j\rangle = -j |j, -j\rangle$. We parametrize α, z as [80, 81]

$$\alpha = \sqrt{\frac{j}{2}}(q + ip), \quad z = \sqrt{\frac{1+P}{1-P}} e^{iQ}, \quad (15)$$

where $(p, q) \in \mathbb{R}^2$ are the canonical variables of the bosonic sector, while $(P, Q) \in \mathbb{R}^2$ with $-1 \leq P \leq 1$, $-\pi \leq Q \leq \pi$ represent the canonical variables of the atomic sector. Then, the classical Hamiltonian of the Dicke model can be written as

$$\mathcal{H}_D^c = \frac{\langle CS|H_D|CS \rangle}{j} = \omega_0 P + \frac{\omega}{2}(p^2 + q^2) + 2\xi q \cos Q \sqrt{1 - P^2}. \quad (16)$$

Consequently, the classical equations of motion (CEM) are given by

$$\begin{aligned} \dot{q} &= \omega p, \quad \dot{p} = -\omega q - 2\xi \cos Q \sqrt{1 - P^2}, \\ \dot{Q} &= \omega_0 - \frac{2\xi q P \cos Q}{\sqrt{1 - P^2}}, \quad \dot{P} = 2\xi q \sin Q \sqrt{1 - P^2}. \end{aligned} \quad (17)$$

with the initial condition (p_0, q_0, P_0, Q_0) .

The chaos presented by \mathcal{H}_D^c in (16) with increasing ξ can be uncovered using the Poincaré section. To define the Poincaré section at certain energy \mathcal{E} , we consider a plane with $p = 0$. As the energy of the system is conserved, i. e. $\mathcal{H}_D^c(p = 0, q, P, Q) = \mathcal{E}$, this plane is actually characterized by the variables (P, Q) . The Poincaré section is then defined as the intersection of the classical trajectories with this surface.

In Figs. 4(b1)-4(b3), we plot Poincaré sections for different values of ξ with energy $\mathcal{E} = 1.2$. For smaller values of ξ , such as the one shown in Fig. 4(b1), the Poincaré section is dominated by regular structure, indicating the regular dynamics in the classical Dicke model. This is in good agreement with quantum case in Fig. 4(a1). When the value of ξ increases the chaotic trajectories appear, leading to a mixed Poincaré section in which the regular islands are coexisting with a chaotic sea, as exemplified in Fig. 4(b2) for the case of $\xi = 2.3$. As ξ is further increased, e. g. $\xi = 1$ case depicted in Fig. 4(b3), the Poincaré section is fully covered by chaotic trajectories, although there may still exist several invisible regular islands.

To quantify the chaotic behavior in the Dicke model, we consider the phase space averaged Lyapunov exponent, defined by

$$\Upsilon_m = \int u_m(P, Q) d\mathcal{A}, \quad (18)$$

where $d\mathcal{A} = dP dQ$ is the area element of the phase space. Here, $u_m(P, Q)$ is the largest Lyapunov exponent and can be calculated through the numerical approach in Refs. [82, 102]. In Fig. 4(b4), we plot Υ_m as a function of ξ with $\mathcal{E} = 1.2$. For small values of ξ , Υ_m stays vanishingly small until $\xi \sim 0.2$, from which it starts to grow as ξ is increased, indicating the onset of chaos. It is worth pointing out that the behavior of $\langle \overline{r} \rangle$ is in good agreement with Υ_m .

Different from the KT model, the classical dynamics of the Dicke model depends on the energy of the model. This requires us to consider the energy shell in which the underlying classical dynamics should not be changed. The energy shell studied in this work is defined by $E_k \in [\bar{E} - 0.15, \bar{E} + 0.02]$ with $\bar{E} = 1.2$. We have checked that there are no substantial variations in the corresponding classical dynamics for this energy interval. Moreover, we would also like to point out that our main results still hold for other choice of energy shells, as long as the classical dynamics keeps unchanged in the chosen energy shell.

Here, we see again a good correspondence between the classical and quantum chaotic features in the Dicke model. As we have pointed out in the KT model, this correspondence is expected in the infinite time limit. In order to get more insights into the correspondence principle in the studies of quantum chaos, it is also necessary to explore the connection between the quantum and classical chaotic properties in the finite time.

A. Dynamical chaos in Dicke model

As we have done in the KT model, the chaoticity of the finite time trajectories in the Dicke model is also measured through the characters of the points in the Poincaré section. However, different from the KT model, the classical dynamics of the Dicke model is governed by the differential equations, rather than the mapping. Hence, it is required to determine how many points of a classical trajectory evolved up to time T_m are taken in the Poincaré section. By defining the time between two successive crossings of the Poincaré section as the traversal time T_r , the number of points in the Poincaré section for a trajectory with T_m iterations is $N_m = T_m/T_r$.

Similar to the KT model, the distribution features of these N_m points in the Poincaré section depend on the chaoticity of the trajectory. To analyze the chaotic behavior of a finite time trajectory, we also discretize the Poincaré section into a grid of M_d cells, and count how many cells are occupied for a given trajectory. This means that there

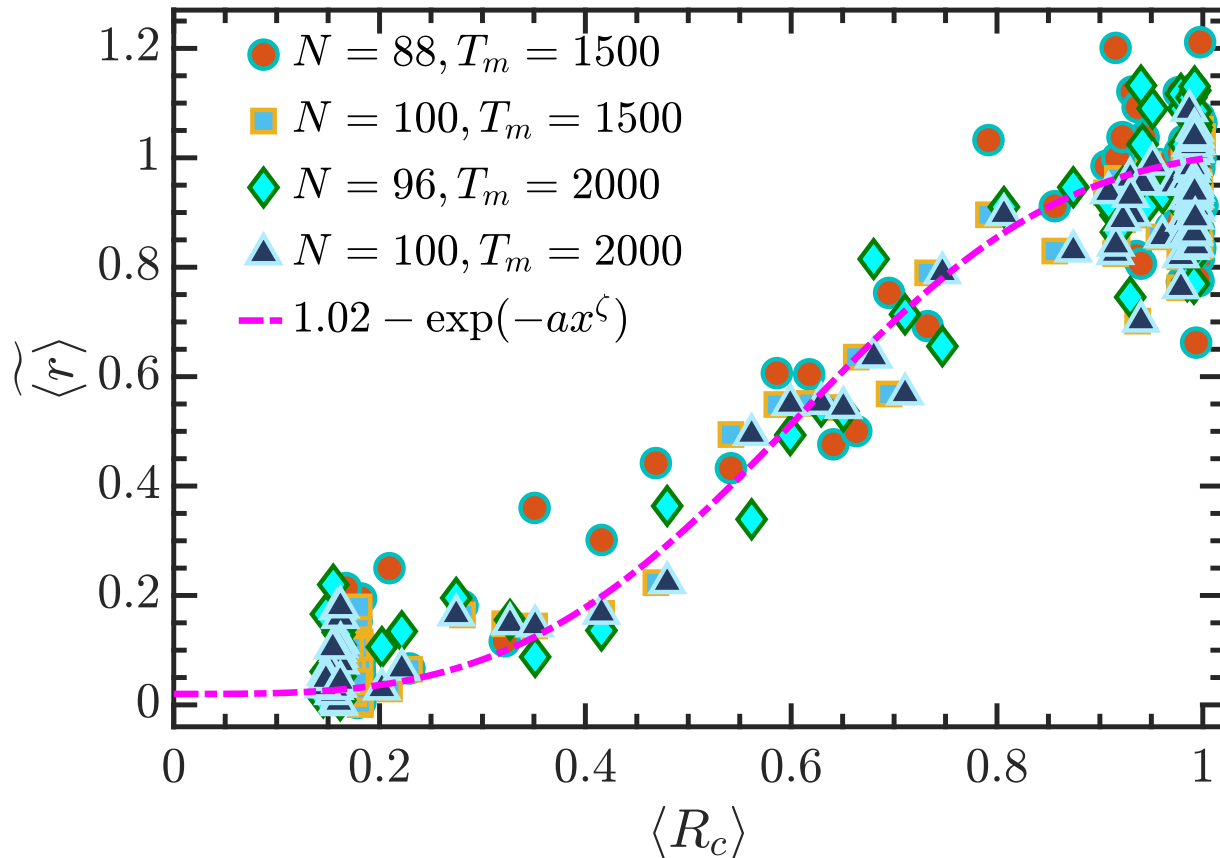


FIG. 6. Quantum chaotic measure $\langle \widetilde{r} \rangle$ in (5) as a function of the finite time classical chaotic measure R_c in (21) for the Dicke model with several values of the system sizes N and T_m . Here, T_m is the evolution time of the classical trajectories and R_c is calculated by averaging over an ensemble with 1600 initial conditions. Moreover, $\langle \widetilde{r} \rangle$ are calculated for the energy levels that satisfy $E \in [\bar{E} - 0.15, \bar{E} + 0.02]$ with $\bar{E} = 1.2$. The magenta dot-dashed curve denotes the best fitting of the data and it has the form $y = 1.02 - \exp(-ax^\zeta)$ with $\zeta \approx 3.3885$ and $a \approx 3.8328$. Other parameters: $\omega = \omega_0 = 1$.

exists an optimal value of M_d . Following the same discussion as in the KT model, it is easy to show that the best choice of M_d is given by $M_d = N_m / \ln 2 \simeq N_m$. We thus define the chaotic measure of a finite time trajectory as

$$R_c = \frac{N_R}{N_m}, \quad (19)$$

where $N_R = M_R / (pM_d)N_m$ with M_R being the number of occupied cells and $p = 1 - (1 - 1/M_d)^{N_m}$.

Let us first focus on the distribution of R_c for an ensemble of initial conditions, defined by

$$P_D(R_c) = \frac{1}{\mathcal{M}_s} \sum_{v=1}^{\mathcal{M}_s} \delta(R_c - R_{c,v}), \quad (20)$$

where \mathcal{M}_s denotes the number of initial conditions in an ensemble. The variation of $P_D(R_c)$ for an ensemble of 1600 initial conditions with different values of ξ and T_m has been illustrated in Fig. 5. An overall similarities between Fig. 2 and Fig. 5 can be clearly identified. Specifically, since the points in the Poincaré section are clustered for the trajectories with regular dynamics, the distribution $P_D(R_c)$ is supported over the smaller values of R_c and its width decreases with increasing T_m , as seen in the first column of Fig. 5. This behavior of $P_D(R_c)$ leads us to expect that it would turn to $P_D(R_c) = \delta(R_c)$ as T_m goes to infinity, and the same trend is also presented in the KT model. On the contrary, as the trajectories with chaotic dynamics result in randomly scattered points in Poincaré section, $P_D(R_c)$ is well described by a narrow distribution around $R_c \simeq 1$, as shown in the last column of Fig. 5. We further note that the distribution of R_c for the chaotic trajectories becomes more and more narrow as T_m is increased, suggesting

$P_D(R_c)$ approaches a delta distribution centered at $R_c = 1$ in the $T_m \rightarrow \infty$ limit, as exhibited by the KT model. The coexistence of the regular and chaotic trajectories in the mixed regime gives rise to the double peak shape of $P_D(R_c)$, as demonstrated in the middle column of Fig. 5. As observed in the KT model, the smoothness of $P_D(R_c)$ can be improved by enhancing T_m .

After verifying the ability of R_c in (19) to capture the chaotic degree of the finite time trajectories, we continue to analyze the validity of the quantum-classical correspondence in the Dicke model for finite time trajectories. According to the results in the KT model, the chaoticity of the classical Dicke model in finite time can be measured by averaging R_c over an ensemble,

$$\langle R_c \rangle = \sum_{v=1}^{\mathcal{M}_s} R_{c,v} P_D(R_c), \quad (21)$$

while the degree of quantum chaos is quantified through $\widetilde{\langle r \rangle}$ [cf. Eq. (5)] in a given energy shell. The correspondence between the quantum and classical chaoticity measures indicates that the variation of $\widetilde{\langle r \rangle}$ should depend strongly on $\langle R_c \rangle$.

The variation of $\widetilde{\langle r \rangle}$ as a function of $\langle R_c \rangle$ for several system sizes N and evolution times T_m in the Dicke model is shown in Fig. 6. The resemblance between Figs. 3 and 6 is clearly visible. However, as the system size and evolution time that can be approached in our numerical simulation of the Dicke model are much smaller than in the KT model, the results for the Dicke model have larger fluctuations, as compared to Fig. 3. Nevertheless, one can see that the fluctuations can be suppressed by increasing N and/or T_m . In particular, as marked by the magenta dot-dashed curve in Fig. 6, the dependence of $\widetilde{\langle r \rangle}$ on $\langle R_c \rangle$ is captured by the same function as in the KT model, i. e. $y = 1.02 - \exp(-ax^\zeta)$. For the Dicke model, we obtain $\zeta \simeq 3.3885, a = 3.8328$, which are remarkably close to the corresponding values in the KT model. Almost the same relationship between the quantum and classical chaotic measures has been observed in two totally different quantum systems. This fact not only confirms that the correspondence principle also holds for the finite time trajectories, but also leads us to expect that our main findings may still be valid for other quantum many-body systems with well-defined classical limit.

IV. CONCLUSIONS

In this work, we have studied how to measure the degree of chaos for finite time trajectories and examined the quantum-classical correspondence in two different quantum systems, namely kicked top and Dicke models. By utilizing the distinct features exhibited by the regular and chaotic trajectories in the Poincaré section, we have shown how to quantify the degree of chaos for a finite time classical trajectory. The correctness of our defined finite time chaotic measure has been verified through a detailed analysis of its probability distribution in our considered models. We have demonstrated that the transition to chaos leaves a strong imprint on the statistical properties of the finite time chaotic measure. Identifying the average of level spacing ratio as the measure of quantum chaos, we have explored the correspondence between the quantum and finite time classical chaoticities in both kicked top and Dicke models. Notably, the dependence of quantum chaotic measure on its classical counterpart can be well described by a simple function, which is independent of the model.

Our findings shed more light on the meaning of quantum-classical correspondence and provide a quantitative way to understand how the chaos develops with increasing time. The analytical expression of the relation between quantum and classical chaotic measures is independent of specific model. This indicates a general standard for ascertaining the quantum-classical correspondence. Moreover, the results of this work not only extend the conclusions of previous work [25], but also enhance our comprehending of quantum statistical physics.

A natural extension of the present work is to systematically investigate whether the quantum and finite time classical chaotic measures have the same relationship as in this work also in other quantum systems with well-defined classical counterpart. We expect that the results of these explorations will align with our conclusions. Another interesting question should be the analytical explanation of why the quantum chaotic measure exhibits the same dependence on the classical measure for different models. It would also be intriguing to examine how the finite time chaotic measure links to other quantum chaotic indicators and particularly the dynamical ones, such as spectral form factor [105] and Krylov complexity [106, 107].

ACKNOWLEDGMENTS

This work was supported by the Slovenian Research and Innovation Agency (ARIS) under the Grants Nos. J1-4387 and P1-0306.

-
- [1] N. Bohr, *Zeitschrift für Physik* **2**, 423 (1920).
- [2] J. Nielsen, *The Correspondence Principle (1918 - 1923)*, ISSN (Elsevier Science, 2013).
- [3] J. Wilkie and P. Brumer, *Phys. Rev. A* **55**, 27 (1997).
- [4] J. Wilkie and P. Brumer, *Phys. Rev. A* **55**, 43 (1997).
- [5] J. B. Keller, *Annals of Physics* **4**, 180 (1958).
- [6] M. Kryvohuz and J. Cao, *Phys. Rev. Lett.* **95**, 180405 (2005).
- [7] M. Gutzwiller, *Chaos in Classical and Quantum Mechanics*, Interdisciplinary Applied Mathematics (Springer New York, 2013).
- [8] C. Jarzynski, H. T. Quan, and S. Rahav, *Phys. Rev. X* **5**, 031038 (2015).
- [9] M. Kumari and S. Ghose, *Phys. Rev. E* **97**, 052209 (2018).
- [10] J. Wang, G. Benenti, G. Casati, and W.-g. Wang, *Phys. Rev. Res.* **2**, 043178 (2020).
- [11] F. J. Arranz, R. M. Benito, and F. Borondo, *Phys. Rev. E* **103**, 062207 (2021).
- [12] B. Vijaywargia and A. Lakshminarayan, “Quantum-classical correspondence in quantum channels,” (2024), arXiv:2407.14067 [quant-ph].
- [13] P. Gaspard, *International Journal of Modern Physics B* **15**, 209 (2001), <https://doi.org/10.1142/S021797920100437X>.
- [14] M. Toda, S. Adachi, and K. Ikeda, *Progress of Theoretical Physics Supplement* **98**, 323 (1989), <https://academic.oup.com/ptps/article-pdf/doi/10.1143/PTPS.98.323/5369276/98-323.pdf>.
- [15] F. Borgonovi, G. Casati, and B. Li, *Phys. Rev. Lett.* **77**, 4744 (1996).
- [16] D. Neilson and R. Bishop, *Recent Progress In Many-body Theories - Proceedings Of The 9th International Conference*, Series On Advances In Quantum Many-body Theory (World Scientific Publishing Company, 1998).
- [17] B. Batistić and M. Robnik, *Phys. Rev. E* **88**, 052913 (2013).
- [18] J. Wang, G. Benenti, G. Casati, and W. ge Wang, *Journal of Physics A: Mathematical and Theoretical* **55**, 234002 (2022).
- [19] Č. Lozej, G. Casati, and T. Prosen, *Phys. Rev. Res.* **4**, 013138 (2022).
- [20] E. G. Altmann, A. E. Motter, and H. Kantz, *Chaos: An Interdisciplinary Journal of Nonlinear Science* **15**, 033105 (2005), https://pubs.aip.org/aip/cha/article-pdf/doi/10.1063/1.1979211/14598327/033105_1_online.pdf.
- [21] J. Wang, G. Casati, and T. Prosen, *Phys. Rev. E* **89**, 042918 (2014).
- [22] J. Huang and H. Zhao, *Phys. Rev. E* **95**, 032209 (2017).
- [23] Č. Lozej, D. Lukman, and M. Robnik, *Phys. Rev. E* **103**, 012204 (2021).
- [24] K. Zahradova, J. Slipantschuk, O. F. Bandtlow, and W. Just, *Phys. Rev. E* **105**, L012201 (2022).
- [25] Z.-Q. Chen, R.-H. Ni, Y. Song, L. Huang, J. Wang, and G. Casati, “The correspondence principle and dynamical chaos,” In preparing.
- [26] F. Haake, S. Gnutzmann, and M. Kuš, *Quantum Signatures of Chaos*, Springer Series in Synergetics (Springer International Publishing, 2019).
- [27] R. H. Dicke, *Phys. Rev.* **93**, 99 (1954).
- [28] F. Haake, M. Kuš, and R. Scharf, *Zeitschrift für Physik B Condensed Matter* **65**, 381 (1987).
- [29] G. M. D’Ariano, L. R. Evangelista, and M. Saraceno, *Phys. Rev. A* **45**, 3646 (1992).
- [30] R. F. Fox and T. C. Elston, *Phys. Rev. E* **50**, 2553 (1994).
- [31] J. N. Bandyopadhyay and A. Lakshminarayan, *Phys. Rev. E* **69**, 016201 (2004).
- [32] S. Ghose, R. Stock, P. Jessen, R. Lal, and A. Silberfarb, *Phys. Rev. A* **78**, 042318 (2008).
- [33] M. Lombardi and A. Matzkin, *Phys. Rev. E* **83**, 016207 (2011).
- [34] S. Dogra, V. Madhok, and A. Lakshminarayan, *Phys. Rev. E* **99**, 062217 (2019).
- [35] T. Herrmann, M. F. I. Kieler, F. Fritzsche, and A. Bäcker, *Phys. Rev. E* **101**, 022221 (2020).
- [36] T. Olsacher, L. Pastori, C. Kokail, L. M. Sieberer, and P. Zoller, *Journal of Physics A: Mathematical and Theoretical* **55**, 334003 (2022).
- [37] Q. Wang and M. Robnik, *Phys. Rev. E* **107**, 054213 (2023).
- [38] A. Anand, R. B. Mann, and S. Ghose, “Non-linearity and chaos in the kicked top,” (2024), arXiv:2408.05869 [nlin.CD].
- [39] M. P. Strzys, E. M. Graefe, and H. J. Korsch, *New Journal of Physics* **10**, 013024 (2008).
- [40] V. M. Bastidas, P. Pérez-Fernández, M. Vogl, and T. Brandes, *Phys. Rev. Lett.* **112**, 140408 (2014).
- [41] U. T. Bhosale and M. S. Santhanam, *Phys. Rev. E* **98**, 052228 (2018).
- [42] L. M. Sieberer, T. Olsacher, A. Elben, M. Heyl, P. Hauke, F. Haake, and P. Zoller, *npj Quantum Information* **5**, 78 (2019).
- [43] D. Mondal, S. Sinha, and S. Sinha, *Phys. Rev. E* **104**, 024217 (2021).
- [44] M. H. Muñoz Arias, P. M. Poggi, and I. H. Deutsch, *Phys. Rev. E* **103**, 052212 (2021).
- [45] C. Yin and A. Lucas, *Phys. Rev. A* **103**, 042414 (2021).
- [46] J. R. G. Alonso, N. Shammah, S. Ahmed, F. Nori, and J. Dressel, “Diagnosing quantum chaos with out-of-time-ordered-correlator quasiparticles,” (2022), arXiv:2201.08175 [quant-ph].
- [47] Q. Wang and M. Robnik, *Phys. Rev. E* **108**, 054217 (2023).

- [48] A. Anand, J. Davis, and S. Ghose, *Phys. Rev. Res.* **6**, 023120 (2024).
- [49] G. Passarelli, P. Lucignano, D. Rossini, and A. Russomanno, “Chaos and magic in the dissipative quantum kicked top,” (2024), [arXiv:2406.16585](https://arxiv.org/abs/2406.16585) [quant-ph].
- [50] S. Chaudhury, A. Smith, B. E. Anderson, S. Ghose, and P. S. Jessen, *Nature* **461**, 768 (2009).
- [51] V. R. Krithika, V. S. Anjusha, U. T. Bhosale, and T. S. Mahesh, *Phys. Rev. E* **99**, 032219 (2019).
- [52] E. J. Meier, J. Ang’ong’a, F. A. An, and B. Gadway, *Phys. Rev. A* **100**, 013623 (2019).
- [53] X. Wang, S. Ghose, B. C. Sanders, and B. Hu, *Phys. Rev. E* **70**, 016217 (2004).
- [54] A. Piga, M. Lewenstein, and J. Q. Quach, *Phys. Rev. E* **99**, 032213 (2019).
- [55] A. Lerose and S. Pappalardi, *Phys. Rev. A* **102**, 032404 (2020).
- [56] V. Oganesyan and D. A. Huse, *Phys. Rev. B* **75**, 155111 (2007).
- [57] Y. Y. Atas, E. Bogomolny, O. Giraud, and G. Roux, *Phys. Rev. Lett.* **110**, 084101 (2013).
- [58] Y. Y. Atas, E. Bogomolny, O. Giraud, P. Vivo, and E. Vivo, *Journal of Physics A: Mathematical and Theoretical* **46**, 355204 (2013).
- [59] O. Giraud, N. Macé, E. Vernier, and F. Alet, *Phys. Rev. X* **12**, 011006 (2022).
- [60] T. Parker and L. Chua, *Practical Numerical Algorithms for Chaotic Systems* (Springer New York, 2012).
- [61] Q. Wang and M. Robnik, *Entropy* **23** (2021), 10.3390/e23101347.
- [62] B. M. Garraway, *Philosophical Transactions of the Royal Society A: Mathematical, Physical and Engineering Sciences* **369**, 1137 (2011), <https://royalsocietypublishing.org/doi/pdf/10.1098/rsta.2010.0333>.
- [63] Y. K. Wang and F. T. Hioe, *Phys. Rev. A* **7**, 831 (1973).
- [64] J. Vidal and S. Dusuel, *Europhysics Letters* **74**, 817 (2006).
- [65] V. M. Bastidas, C. Emary, B. Regler, and T. Brandes, *Phys. Rev. Lett.* **108**, 043003 (2012).
- [66] L. Bakemeier, A. Alvermann, and H. Fehske, *Phys. Rev. A* **85**, 043821 (2012).
- [67] O. Castaños, E. Nahmad-Achar, R. López-Peña, and J. G. Hirsch, *Phys. Rev. A* **86**, 023814 (2012).
- [68] T. Brandes, *Phys. Rev. E* **88**, 032133 (2013).
- [69] P. Pérez-Fernández and A. Relaño, *Phys. Rev. E* **96**, 012121 (2017).
- [70] K. Gietka and T. Busch, *Phys. Rev. E* **104**, 034132 (2021).
- [71] R. J. Lewis-Swan, S. R. Muleady, D. Barberena, J. J. Bollinger, and A. M. Rey, *Phys. Rev. Res.* **3**, L022020 (2021).
- [72] A. L. Corps and A. Relaño, *Phys. Rev. Lett.* **127**, 130602 (2021).
- [73] P. Das and A. Sharma, *Phys. Rev. A* **105**, 033716 (2022).
- [74] P. Das, D. S. Bhakuni, and A. Sharma, *Phys. Rev. A* **107**, 043706 (2023).
- [75] C. M. Lóbez and A. Relaño, *Phys. Rev. E* **94**, 012140 (2016).
- [76] C. Emary and T. Brandes, *Phys. Rev. E* **67**, 066203 (2003).
- [77] C. Emary and T. Brandes, *Phys. Rev. Lett.* **90**, 044101 (2003).
- [78] A. Altland and F. Haake, *New Journal of Physics* **14**, 073011 (2012).
- [79] X.-W. Hou and B. Hu, *Phys. Rev. A* **69**, 042110 (2004).
- [80] M. A. Bastarrachea-Magnani, B. L. del Carpio, S. Lerma-Hernández, and J. G. Hirsch, *Physica Scripta* **90**, 068015 (2015).
- [81] M. A. Bastarrachea-Magnani, B. López-del Carpio, J. Chávez-Carlos, S. Lerma-Hernández, and J. G. Hirsch, *Phys. Rev. E* **93**, 022215 (2016).
- [82] J. Chávez-Carlos, M. A. Bastarrachea-Magnani, S. Lerma-Hernández, and J. G. Hirsch, *Phys. Rev. E* **94**, 022209 (2016).
- [83] W. Buijsman, V. Gritsev, and R. Sprik, *Phys. Rev. Lett.* **118**, 080601 (2017).
- [84] S. Lerma-Hernández, D. Villaseñor, M. A. Bastarrachea-Magnani, E. J. Torres-Herrera, L. F. Santos, and J. G. Hirsch, *Phys. Rev. E* **100**, 012218 (2019).
- [85] Q. Wang and M. Robnik, *Phys. Rev. E* **102**, 032212 (2020).
- [86] D. Villaseñor, S. Pilatowsky-Cameo, M. A. Bastarrachea-Magnani, S. Lerma-Hernández, L. F. Santos, and J. G. Hirsch, *New Journal of Physics* **22**, 063036 (2020).
- [87] D. Villaseñor, S. Pilatowsky-Cameo, M. A. Bastarrachea-Magnani, S. Lerma-Hernández, L. F. Santos, and J. G. Hirsch, *Entropy* **25** (2023), 10.3390/e25010008.
- [88] A. V. Kirkova and P. A. Ivanov, *Physica Scripta* **98**, 045105 (2023).
- [89] D. Tiwari and S. Banerjee, *Proceedings of the Royal Society A: Mathematical, Physical and Engineering Sciences* **479**, 20230431 (2023), <https://royalsocietypublishing.org/doi/pdf/10.1098/rspa.2023.0431>.
- [90] Y. Alavirad and A. Lavasani, *Phys. Rev. A* **99**, 043602 (2019).
- [91] R. J. Lewis-Swan, A. Safavi-Naini, J. J. Bollinger, and A. M. Rey, *Nature Communications* **10**, 1581 (2019).
- [92] K. Baumann, C. Guerlin, F. Brennecke, and T. Esslinger, *Nature* **464**, 1301 (2010).
- [93] Z. Zhang, C. H. Lee, R. Kumar, K. J. Arnold, S. J. Masson, A. L. Grimsmo, A. S. Parkins, and M. D. Barrett, *Phys. Rev. A* **97**, 043858 (2018).
- [94] P. Kirton, M. M. Roses, J. Keeling, and E. G. Dalla Torre, *Advanced Quantum Technologies* **2**, 1800043 (2019), <https://onlinelibrary.wiley.com/doi/pdf/10.1002/qute.201800043>.
- [95] D. Villaseñor, S. Pilatowsky-Cameo, J. Chávez-Carlos, M. A. Bastarrachea-Magnani, S. Lerma-Hernández, L. F. Santos, and J. G. Hirsch, “Classical and quantum properties of the spin-boson dicke model: Chaos, localization, and scarring,” (2024), [arXiv:2405.20381](https://arxiv.org/abs/2405.20381) [quant-ph].
- [96] M. A. Bastarrachea-Magnani, S. Lerma-Hernández, and J. G. Hirsch, *Phys. Rev. A* **89**, 032102 (2014).
- [97] M. A. Bastarrachea-Magnani, D. Villaseñor, J. Chávez-Carlos, S. Lerma-Hernández, L. F. Santos, and J. G. Hirsch, *Phys. Rev. E* **109**, 034202 (2024).
- [98] K. Furuya, M. C. Nemes, and G. Q. Pellegrino, *Phys. Rev. Lett.* **80**, 5524 (1998).
- [99] L. Song, D. Yan, J. Ma, and X. Wang, *Phys. Rev. E* **79**, 046220 (2009).

- [100] U. Bhattacharya, S. Dasgupta, and A. Dutta, *Phys. Rev. E* **90**, 022920 (2014).
- [101] J. Chávez-Carlos, B. López-del Carpio, M. A. Bastarrachea-Magnani, P. Stránský, S. Lerma-Hernández, L. F. Santos, and J. G. Hirsch, *Phys. Rev. Lett.* **122**, 024101 (2019).
- [102] Q. Wang and M. Robnik, *Phys. Rev. E* **109**, 024225 (2024).
- [103] M. de Aguiar, K. Furuya, C. Lewenkopf, and M. Nemes, *Annals of Physics* **216**, 291 (1992).
- [104] W.-M. Zhang, D. H. Feng, and R. Gilmore, *Rev. Mod. Phys.* **62**, 867 (1990).
- [105] P. Kos, M. Ljubotina, and T. Prosen, *Phys. Rev. X* **8**, 021062 (2018).
- [106] D. E. Parker, X. Cao, A. Avdoshkin, T. Scaffidi, and E. Altman, *Phys. Rev. X* **9**, 041017 (2019).
- [107] V. Balasubramanian, P. Caputa, J. M. Magan, and Q. Wu, *Phys. Rev. D* **106**, 046007 (2022).